

Impact of surface doping profile and passivation layers on surface-related degradation in silicon PERC solar cells

Chandany Sen ^{a,*}, Phillip Hamer ^a, Anastasia Soeriyadi ^a, Brendan Wright ^a, Matthew Wright ^a, Aref Samadi ^a, Daniel Chen ^a, Bruno Vicari Stefani ^a, Daqi Zhang ^b, Jian Wu ^b, Fangdan Jiang ^b, Brett Hallam ^a, Malcolm Abbott ^a

^a School of Photovoltaic and Renewable Energy Engineering, University of New South Wales, Sydney, NSW, 2052, Australia

^b Canada Solar Inc., Suzhou, 215562, China



ARTICLE INFO

Keywords:

Surface-related degradation
Emitter doping profile
Surface passivation
Thermal oxides
Light soaking
p-type silicon

ABSTRACT

Illuminated solar cells are susceptible to various degradation mechanisms that can act to reduce the total energy yield when deployed. One potentially severe form is an increase in carrier recombination in the surface regions. This effect has been reported at both the undoped rear surface and phosphorous diffused emitter of PERC solar cells. This work investigates the influence of a range of surface conditions on the surface-related degradation (SRD) behaviour in PERC solar cells. It is shown that SRD is strongly affected by the doping profile of phosphorous emitters, the use of thin thermal oxides with $\text{SiN}_x:\text{H}$ dielectric passivation layers, the substrate material, and the configuration of the rear surface passivation. It finds that more lightly doped emitters result in more front side SRD, with its extent increasing with the introduction of the $\text{SiO}_2/\text{SiN}_x:\text{H}$ surface passivation layers. Czochralski silicon (Cz-Si) wafers were observed to be significantly more susceptible to surface degradation than multi-crystalline silicon (mc-Si) wafers, which we attribute to less trapping of hydrogen in the bulk of those substrates. On the rear side of PERC cells, surface degradation was only observed in structures that incorporated the combination of $\text{SiO}_2/\text{SiN}_x:\text{H}$ rear layers. No SRD was observed in the existing $\text{Al}_2\text{O}_3/\text{SiN}_x:\text{H}$ technology used in the industrial PERC cells studied. However, the results presented have implications for future commercial solar cell technologies, which are transitioning towards lightly doped emitters and commonly incorporate thermal oxides for surface passivation.

1. Introduction

The silicon wafer-based passivated emitter and rear cell (PERC) technology currently dominates global production with over 85% market share [1]. However, the cell architecture is potentially subject to a range of bulk- [2–17] and surface-related degradation mechanisms [18–22], which are commonly accelerated by temperature and carrier injection. These degradation modes can cause severe power loss and thus represent a challenge for silicon solar cell manufacturers. For the last few decades, research has focussed on bulk related degradation (BRD). Academia and industry have given much attention to both the boron-oxygen defect (BO) [5–9,17] and light- and elevated temperature-induced degradation (LeTID) [2,3,10–16,23–25]. These problems are now relatively well understood, and manufacturing solutions (including dedicated tools for mitigation) now exist. Testing

standards are also in place to identify susceptible solar cells. However, there have also been reports that light-induced degradation may also occur in the surface regions herein called surface-related degradation (SRD). Such degradation tends to occur over a much longer timescale, in some cases, effects are only observable after ≥ 1000 h [26–28]. This has meant there are relatively few published studies on this effect; it is concerning for industry since it may not be detected by standard stability testing procedures (which typically target BRD). PERC solar cells rely on the outstanding electrical performance of both surfaces, and as wafer quality improves, maintaining high-quality surface passivation becomes critical. This paper examines the problem of long-term surface stability on both the front side and rear side of PERC type solar cells. Specifically, it studies the role of substrate, emitter doping profile and surface layer types on the magnitude of surface degradation.

There have been several reports of surface degradation in both PERC

* Corresponding author.

E-mail address: chandany.sen@unsw.edu.au (C. Sen).

cells and test structures that approximate parts of that structure. Table 1 presents a summary of the structures tested, the nature of the degradation, and the testing conditions used.

From the table, it can be determined that both substrate materials and surface conditions play a role in varying the extent of SRD. A more pronounced SRD has been observed on FZ-Si as compared to Cz-Si [26–28]. However, it remains unclear if SRD impacts Cz-Si more or less when compared to mc-Si material since there has only been one report on mc-Si wafers [26]. SRD was observed to impact samples with both doped and undoped surfaces [20,21,26–28,30,31], indicating that both front and rear sides of PERC cells are potentially susceptible to surface related-degradation. Several studies measured SRD on heavily doped surfaces (sheet resistance of $\sim 28\text{--}78 \Omega/\square$) [21,31]; however, there has as yet been no systematic investigation of how varying emitter sheet resistance impacts the extent of SRD. According to the most recent ITRPV report, industrial silicon solar cells have gradually moved towards more lightly doped emitters to reduce emitter saturation current density and improve cell efficiency [1]. Therefore, it is essential to understand if this progression will substantially be affected by SRD on the front side. In non-diffused samples, severe SRD was realized in the structures with silicon dioxide/hydrogenated silicon nitride ($\text{SiO}_2/\text{SiN}_x:\text{H}$) surface passivation [21,26,27], which resulted in $\sim 10\%\text{abs}$ loss in efficiency when applied to the rear side of PERC cells [29]. However, it remains an open question if this is the case in PERC cells that use hydrogenated aluminium oxide/hydrogenated silicon nitride ($\text{Al}_2\text{O}_3/\text{SiN}_x:\text{H}$) rear passivation layers and if modifying the thickness of any passivation types will influence the extent of SRD.

In this work, we examine the role of 4 critical elements of solar cell design on SRD:

- 1) The emitter phosphorus diffusion profile,
- 2) The use of $\text{SiN}_x:\text{H}$ and $\text{SiO}_2/\text{SiN}_x:\text{H}$ surface passivation layers,
- 3) The substrate material, boron-doped (p-type) Cz-Si or mc-Si,

Table 1
Summary of previous studies of surface-related degradation in PERC cells and test structures.

Wafer Type	Front surface	Rear surface	Degradation condition	Degradation impact	Reference
Cells with the emitter on the front side					
Cz-Si p-type (1.3 Ω cm)	n^+ emitter/ $\text{SiN}_x:\text{H}$	$\text{SiO}_2/\text{SiN}_x:\text{H}$	150 °C, 1 sun (~ 555 h)	$V_{\text{OC}}: 20 \text{ mV},$ $\eta: 10\%\text{abs}$	[29]
Lifetime test structures: without emitter on both sides					
FZ-Si p-type (200 Ω cm)	$\text{SiO}_2/\text{SiN}_x:\text{H}$	$\text{SiO}_2/\text{SiN}_x:\text{H}$	80 °C, 1 sun (~ 2000 h)	$J_{\text{oe}}: +1400\%\text{rel}$	[26]
FZ-Si p-type (2 Ω cm)	$\text{SiO}_2/\text{SiN}_x:\text{H}$	$\text{SiO}_2/\text{SiN}_x:\text{H}$	80 °C, 1 sun (~ 2000 h)	$J_{\text{oe}}: +1100\%\text{rel}, \tau_{\text{eff}}: 95\%\text{rel}$	[26]
FZ-Si p-type (2 Ω cm)	$\text{AlO}_x:\text{H}/\text{SiN}_x:\text{H}$	$\text{AlO}_x:\text{H}/\text{SiN}_x:\text{H}$	80 °C, 1 sun (~ 1000 h)	$J_{\text{oe}}: +250\%\text{rel},$ $\tau_{\text{eff}}: 70\%\text{rel}$	[26]
Cz-Si p-type (2 Ω cm)	$\text{SiN}_x:\text{H}$	$\text{SiN}_x:\text{H}$	80 °C, 1 sun (~ 4000 h)	$J_{\text{oe}}: +600\%\text{rel}, \tau_{\text{eff}}: 79\%\text{rel}$	[26]
mc-Si p-type (1 Ω cm)	$\text{SiN}_x:\text{H}$	$\text{SiN}_x:\text{H}$	75 °C, 1 sun (~ 5000 h)	$\tau_{\text{eff}}: 65\%\text{rel}$	[26]
FZ-Si n-type (2.5 Ω cm)	$\text{SiN}_x:\text{H}$	$\text{SiN}_x:\text{H}$	80 °C, 1 sun (~ 2000 h)	$\tau_{\text{eff}}: 75\%\text{rel}$	[28]
Cz-Si p-type (2 Ω cm)	$\text{AlO}_x:\text{H}/\text{SiO}_2/\text{SiN}_x:\text{H}$	$\text{AlO}_x:\text{H}/\text{SiO}_2/\text{SiN}_x:\text{H}$	80 °C, 1 sun (~ 5000 h)	$J_{\text{oe}}: +300\%\text{rel},$ $\tau_{\text{eff}}: 70\%\text{rel}$	[27]
Cz-Si p-type (2 Ω cm)	$\text{SiO}_2/\text{SiN}_x:\text{H}$	$\text{SiO}_2/\text{SiN}_x:\text{H}$	80 °C, 1 sun (~ 1000 h)	$J_{\text{oe}}: +800\%\text{rel},$ $\tau_{\text{eff}}: 82\%\text{rel}$	[27]
Cz-Si p-type (1.7 Ω cm)	$\text{SiN}_x:\text{H}$	$\text{SiN}_x:\text{H}$	175 °C, dark (~ 100 h)	$J_{\text{oe}}: +350\%\text{rel}$ $\tau_{\text{eff}}: 65\%\text{rel}$	[20] ¹
Cz-Si p-type (1.7 Ω cm)	$\text{AlO}_x:\text{H}/\text{SiN}_x:\text{H}$	$\text{AlO}_x:\text{H}/\text{SiN}_x:\text{H}$	175 °C, dark (~ 50 h)	$J_{\text{oe}}: +250\%\text{rel}$ $\tau_{\text{eff}}: 65\%\text{rel}$	[20] ¹
Cz-Si n-type (2 Ω cm)	$\text{SiN}_x:\text{H}$	$\text{SiN}_x:\text{H}$	175 °C, dark (~ 15 h)	$J_{\text{oe}}: +30\%\text{rel}$	[30] ¹
Cz-Si n-type (2.5 Ω cm)	$\text{SiN}_x:\text{H}$	$\text{SiN}_x:\text{H}$	175 °C, 1 sun (~ 300 h)	$J_{\text{oe}}: +120 \text{ fA/cm}^2$	[21]
Cz-Si n-type (2.5 Ω cm)	$\text{SiO}_2/\text{SiN}_x:\text{H}$	$\text{SiO}_2/\text{SiN}_x:\text{H}$	175 °C, 1 sun (~ 1000 h)	$J_{\text{oe}}: +360 \text{ fA/cm}^2$	[21]
Cz-Si p-type (1.9 Ω cm)	$\text{SiN}_x:\text{H}$	$\text{SiN}_x:\text{H}$	175 °C, 1 sun (~ 500 h)	$J_{\text{oe}}: +240 \text{ fA/cm}^2$	[21]
Cz-Si p-type (1.9 Ω cm)	$\text{SiO}_2/\text{SiN}_x:\text{H}$	$\text{SiO}_2/\text{SiN}_x:\text{H}$	175 °C, 1 sun (~ 1000 h)	$J_{\text{oe}}: +340 \text{ fA/cm}^2$	[21]
Lifetime test structures: with the emitter on both sides					
Cz-Si n-type (2 Ω cm)	$p^+(100 \Omega/\square)/\text{SiN}_x:\text{H}$	$p^+(100 \Omega/\square)/\text{SiN}_x:\text{H}$	160 °C, 1 sun (~ 20 h)	$J_{\text{oe}}: +25\%\text{rel}$	[31] ¹
Cz-Si n-type (2 Ω cm)	$n^+(65 \Omega/\square)/\text{SiN}_x:\text{H}$	$n^+(65 \Omega/\square)/\text{SiN}_x:\text{H}$	160 °C, 1 sun (~ 20 h)	$J_{\text{oe}}: +15\%\text{rel}$	[31] ¹
Cz-Si n-type (2.5 Ω cm)	$n^+(28 \Omega/\square)/\text{SiN}_x:\text{H}$	$n^+(28 \Omega/\square)/\text{SiN}_x:\text{H}$	175 °C, 1 sun (~ 300 h)	$J_{\text{oe}}: +60 \text{ fA/cm}^2$	[21]
Cz-Si n-type (2.5 Ω cm)	$n^+(33\Omega/\square)/\text{SiO}_2/\text{SiN}_x:\text{H}$	$n^+(33\Omega/\square)/\text{SiO}_2/\text{SiN}_x:\text{H}$	175 °C, 1 sun (~ 1000 h)	$J_{\text{oe}}: +80 \text{ fA/cm}^2$	[21]
Cz-Si p-type (1.9 Ω cm)	$n^+(62 \Omega/\square)/\text{SiN}_x:\text{H}$	$n^+(62 \Omega/\square)/\text{SiN}_x:\text{H}$	175 °C, 1 sun (~ 300 h)	$J_{\text{oe}}: +90 \text{ fA/cm}^2$	[21]
Cz-Si p-type (1.9 Ω cm)	$n^+(78\Omega/\square)/\text{SiO}_2/\text{SiN}_x:\text{H}$	$n^+(78\Omega/\square)/\text{SiO}_2/\text{SiN}_x:\text{H}$	175 °C, 1 sun (~ 2000 h)	$J_{\text{oe}}: +50 \text{ fA/cm}^2$	[21]

¹Note that these papers were presented by the research group authoring this paper.

- 4) The rear passivation layers by varying the thickness of Al_2O_3 , $\text{SiN}_x:\text{H}$ and SiO_2 films.

These are important, not only for understanding degradation in current cell designs, but for identifying potential degradation that may occur as these design elements evolve into the future, in particular for devices featuring passivated contacts with a heavy reliance on maintaining excellent surface passivation.

2. General methodology

This section describes general methodologies (process conditions and characterization methods) used in all groups in this study, more specific process conditions and experimental flow diagrams will be presented along with the specific results.

Boron-doped silicon wafers (mc-Si, 1.9 Ω cm, and Cz-Si, 1.7 Ω cm) were used for fabricating symmetrical lifetime test structures and PERC cell precursors (i.e., cells with no metal). All wafers underwent acidic texturing (for mc-Si) or alkaline texturing (for Cz-Si) to achieve a final thickness of approximately $180 \pm 2 \mu\text{m}$. Wafers were chemically cleaned using a Radio Corporation of America (RCA) cleaning procedure and HF dip prior to phosphorus diffusion. The formation of n-doped emitters was done using a phosphoryl chloride (POCl_3) source in a quartz tube furnace. $\text{SiN}_x:\text{H}$ passivation layers with a 2.08 refractive index at 633 nm and thickness of ~ 75 nm were deposited using a Meyer Burger MAiA remote plasma-enhanced chemical vapour deposition tool (r-PECVD). The firing was carried out at an actual wafer temperature of 743 ± 3 °C with a belt speed of 4.5 m/min using a commercial infrared firing furnace (Sierratherm). The stability testing was performed at 130 °C with an illumination intensity of 1000 W/m² (measured at the sample level) produced by a halogen lamp. The elevated temperature of 130 °C was selected for this study to accelerate the testing cycle so that SRD could be observed in a reasonable timescale [21,26,32].

For all samples, the minority carrier lifetime measurements were performed (at 30 °C) ex-situ using a quasi-steady-state photoconductance tool (QSS-PC) (Sinton Instruments WCT-120TS) [33] and analyzed using the generalized mode as suggested by Nagel et al. [34]. These measurements were obtained on tokens after firing and after incremental steps during stability testing. The inverse Auger related lifetimes were then subtracted from the measured inverse effective minority carrier lifetime using the Coulomb-enhanced Auger parameterization model proposed by Richter et al. [35]. The effective minority carrier lifetime (τ_{eff}) was extracted at an excess minority carrier density of 10% of the bulk doping density.

To compare the bulk related-degradation behaviour, an apparent normalized defect density (NDD) was used and determined using equation (1) [36].

$$\text{NDD} (t) = \frac{1}{\tau_{\text{eff}}(t)} - \frac{1}{\tau_{\text{eff-fired}}} \quad (1)$$

where $\tau_{\text{eff}}(t)$ represented the effective carrier lifetime after each incremental light soaking, and $\tau_{\text{eff-fired}}$ was the effective carrier lifetime after firing. It should be noted that although the purpose of NDD is to provide a measure of the concentration of bulk defects, the apparent NDD may include changes in both bulk- and surface-related lifetime components.

The emitter saturation current density (J_{0e}) was extracted by fitting injection level dependent lifetimes using equation (2):

$$\frac{1}{\tau_{\text{eff}}} = \frac{1}{\tau_{\text{surf}}} + \frac{1}{\tau_{\text{SRH}}} \quad (2)$$

where τ_{surf} was the surface recombination related lifetime component and τ_{SRH} was the injection-dependent Shockley-Read-Hall (SRH) bulk recombination related lifetime component. The τ_{surf} was assumed to be dependent on the emitter saturation current density J_{0e} , which when applied to samples with symmetric emitters is described by equation (3) [37]:

$$\frac{1}{\tau_{\text{surf}}} = 2J_{0e} \times \frac{(N_A + \Delta n)}{qWn_i^2} \quad (3)$$

where N_A , Δn , n_i , W , and q represented the bulk doping concentration, the excess minority carrier concentration, the intrinsic carrier concentration, the wafer thickness, and the fundamental charge constant, respectively.

The τ_{SRH} was assumed to be a single defect with a single trap level and was determined using equation (4), the fundamental SRH equation as follows [38]:

$$\frac{1}{\tau_{\text{SRH}}} = \frac{np - n_i^2}{\Delta n [\tau_{n0}(n + n_1) + \tau_{p0}(p + p_1)]} \quad (4)$$

where n and p were the total electron and hole concentrations, τ_{n0} and τ_{p0} were the SRH-related electron and hole recombination lifetimes, and n_1 and p_1 were the SRH-related electron and hole populations characteristic of the trap level within the bandgap, respectively. An energy level of mid-gap was chosen to assess the defect characteristics as the exact energy level remains unknown, and a broad range of defect energy levels (with a sufficient distance from the band edges) result in recombination properties similar to that of a mid-gap defect. The fitting was achieved by varying each of J_{0e} , τ_{n0} and τ_{p0} and then minimizing the difference between modelled and measured data using a Chi-squared metric [32].

3. Influence of emitter doping profile and passivation type

A series of samples with varied doping profiles and two commonly used types of surface passivation were created to better understand the increasing recombination within emitter regions. High-performance (HP) p-type mc-Si wafers were selected from neighbouring locations in

the ingot. Samples were diffused with various emitter sheet resistances (R_{sheet}), ranging between $\sim 65 \Omega/\square$ to $\geq 570 \Omega/\square$ on both sides, with the detailed process parameters (number of steps, temperature, flowing gas) presented in Table 2. Subsequently, mc-Si samples were divided into two groups. Group 3.1: Emitter with $\text{SiN}_x:\text{H}$ surface passivation layers; and Group 3.2: Emitter with $\text{SiO}_2/\text{SiN}_x:\text{H}$ surface passivation layers. For Group 3.1, after PSG removal, all samples directly underwent $\text{SiN}_x:\text{H}$ dielectric layer deposition on both sides. For Group 3.2, prior to $\text{SiN}_x:\text{H}$ deposition, SiO_2 layers (10-nm-thick) were grown on both sides using a thermal oxidation process at 890 °C for 15 min. Both groups were then laser cleaved into 52 mm × 52 mm tokens, followed by firing and stability testing. The detailed process flow diagram and the various structures used can be found in Fig. 1.

Fig. 2 presents the active phosphorous concentration as a function of depth from the silicon surface as measured using electrochemical capacitance-voltage (ECV). As illustrated, the introduction of SiO_2 layers through the thermal oxidation process reduced active doping concentration at the surface resulting in a $\sim 20 \Omega/\square$ increase in the emitter sheet resistance for the samples with the initial R_{sheet} between $\sim 65 \Omega/\square$ to $\sim 220 \Omega/\square$. However, for samples with the initial $R_{\text{sheet}} \geq 570 \Omega/\square$, this thermal process caused an increase in R_{sheet} by $\sim 300 \Omega/\square$. According to the multiple measurements on several points on a few wafers (6-inch size), it is noted that for the samples with $R_{\text{sheet}} \sim 65 \Omega/\square$ to $\sim 220 \Omega/\square$, the surface doping concentration/profiles were more uniform across the wafer area. However, for samples with $R_{\text{sheet}} \geq 570 \Omega/\square$, the surface doping profiles were varied across the wafer area due to the relatively low concentration of phosphorous atoms; therefore, the sign “ \geq ” was used for this condition. Also, as shown in Fig. 2, there was a slight decrease in doping concentration at the near-surface region (at $\sim 0.1 \mu\text{m}$ depth) of the ECV profiles of the sample with $R_{\text{sheet}} \geq 870 \Omega/\square$ following the thermal oxidation process (opened downward pink triangle curve), the reason for this was unclear. However, it was likely due to an artifact of the ECV measurement.

3.1. Impact of various emitter doping profiles with $\text{SiN}_x:\text{H}$ on degradation

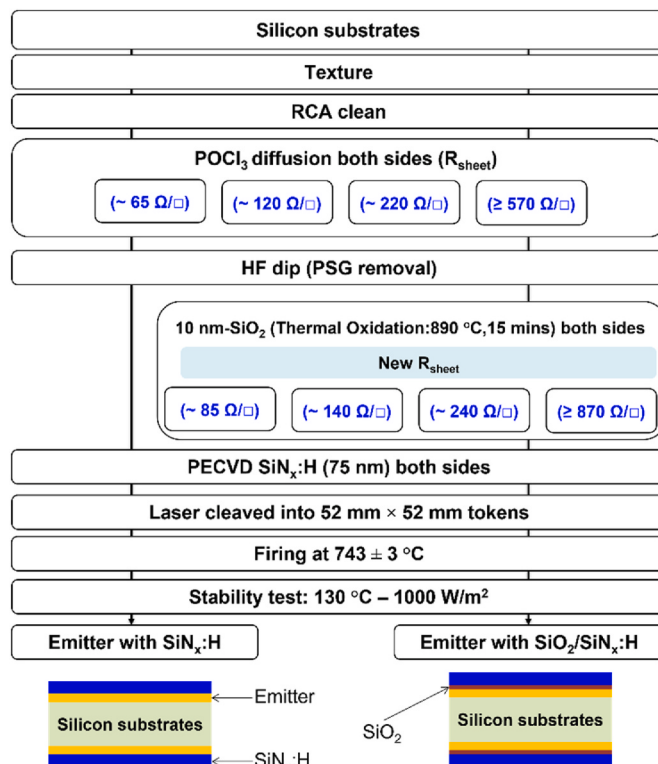
Varying surface diffusion profiles with a $\text{SiN}_x:\text{H}$ surface passivation layer significantly impacted the degradation characteristic, particularly for SRD. Fig. 3 shows the evolution of τ_{eff} and J_{0e} as a function of light soaking duration for mc-Si samples diffused with an emitter sheet resistance of $\sim 65 \Omega/\square$ to $\geq 570 \Omega/\square$ passivated with $\text{SiN}_x:\text{H}$ films. Samples showed initial (after firing) effective lifetimes ranging from $\sim 80 \mu\text{s}$ to $\sim 150 \mu\text{s}$, the differences were mainly due to different extents of surface recombination, see Fig. 3 (c), which depended on the dopant concentration of the emitter layer. However, after $\sim 10 \text{ h}$ of light soaking (the maximum point of degradation), they all dropped to a similar value, $\sim 20 \mu\text{s}$. All samples experienced an initial degradation, followed by a recovery phase. This degradation and recovery were completed after $\sim 60 \text{ h}$ of light soaking. During the first degradation and recovery phases, J_{0e} remained relatively stable (see Fig. 3 (c)). Therefore, this first degradation/regeneration phase is attributed to a form of BRD, likely LeTID, as observed in earlier work [3,39–41].

After the recovery of the bulk lifetime, a second degradation occurred. This degradation manifested as an increase in J_{0e} , which indicates that SRD is occurring (see Fig. 3 (c)), driving increased recombination in the near-surface regions. The mechanism of this degradation could be increased recombination at the interface with the passivation layer, a decrease in the effectiveness of the passivation (e.g., due to a loss of fixed charge) or an increased amount of Shockley-Read-Hall (SRH) recombination within the heavily doped regions itself. Further studies would be required to separate these effects more conclusively.

Although all mc-Si samples in this group were diffused with a range of surface doping profiles, after $\sim 10 \text{ h}$ of light soaking, they had similar NDD of $\sim 4.7 \times 10^{-2}/\mu\text{s}$, see Fig. 3 (b), suggesting that BRD behaviour, likely LeTID, was not significantly different. These results aligned with those of Otaegi et al. [42], showing that the introduction of different

Table 2POCl₃ diffusion process conditions.

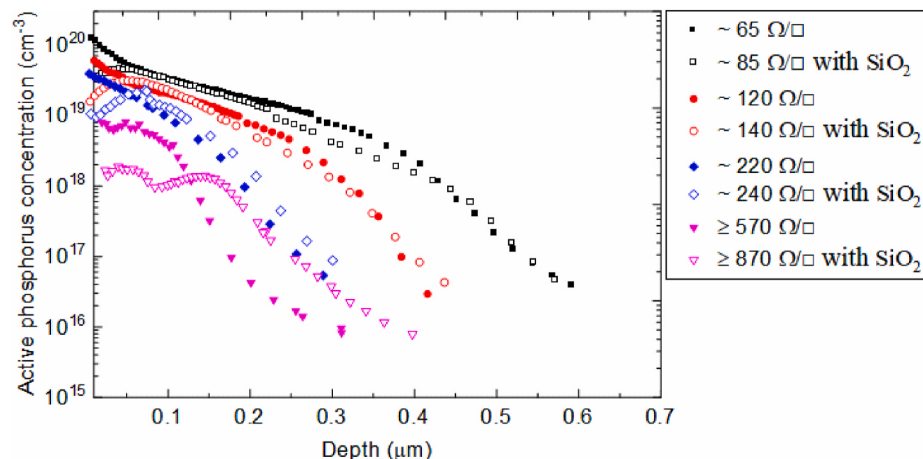
1st step (Pre-deposition)			2nd step (Drive-in)			3rd step (Oxidation-step)			R _{sheet} (Ω/□)
Temp. (°C)	Time (mins)	POCl ₃ /O ₂ /N ₂ (sccm)	Temp. (°C)	Time (min)	N ₂ (slm)	Temp. (°C)	Time (mins)	O ₂ /N ₂ (slm)	
770	25	400/600/6200	850	25	7.5	880	40	5/2.5	~65
770			810			880			~120
760			780			880			~220
730			750			880			≥570

**Fig. 1.** Experiment flow diagram (top) and various sample structures (bottom) for studying the impact of various n⁺ emitter with and without SiO₂.

emitter layers has only a minor impact on the extent of LeTID. However, varying surface doping profiles substantially modulated the extent of SRD, where a greater extent (more significant increase in J_{0e}) was seen on the samples with more lightly doped emitters. No significant surface degradation (J_{0e} remained constant) was observed on the sample with

R_{sheet} ~65 Ω/□. However, after ~2000 h of light soaking, J_{0e} increased from ~34%_{rel} (R_{sheet} ~120 Ω/□) to ~163%_{rel} (R_{sheet} ≥ 570 Ω/□) for all other emitter profiles. It is essential to point out that the stability of the surfaces observed on the sample with R_{sheet} ~65 Ω/□ (J_{0e} remained constant) was not simply due to the higher initial J_{0e} (200 fA/cm²) of this sample, as SRD was still observed for a sample in another group with an initial J_{0e} ≥ 200 fA/cm² (data presented in section 4). Therefore, the stability of the surface region in the sample with R_{sheet} ~65 Ω/□ was mainly due to the presence of a heavy diffusion, in agreement with previous investigations by Sperber et al. [43].

While the precise form of defects causing surface degradation is yet to be identified, it has been proposed that it is likely due to the formation of extended crystallographic defects created due to the accumulation of hydrogen in the near-surface region [20–22,44–47]. Hydrogen is well known to passivate dangling bonds at the interface between the silicon lattice and the surface films [48–51]. However, in the case of the SRD observed in this work, it is thought that too much hydrogen has accumulated in the crystalline silicon close to the surface leading to the formation of extended defects as has been observed and discussed in other studies [20–22,44–47]. Further work involving TEM studies of these failed surface regions may help to confirm this root cause in future studies. More dopants present in the heavily diffused layers may attract more hydrogen, forming P–H pairs, leaving less and/or insignificant free hydrogen to cause SRD. For the lightly diffused surface, there would be less formation of P–H pairs, resulting in more free hydrogen moving to and building up at/near the surface interface region, causing more surface damage. The results in this work raise questions about potential SRD issues in emerging technologies and future solar cells. These include passivated contact architectures (e.g., TOPCon) that utilize diffused junctions residing underneath doped oxide films for enhanced surface passivation as well as solar cells with selective emitters employing sheet resistances at non-contacted regions that projected to increase from ~140 Ω/□ to ~200 Ω/□ [1].

**Fig. 2.** Active phosphorous concentration as a function of depth from the silicon surface as measured using ECV of samples diffused with emitter sheet resistance ranging from ~65 Ω/□ to ≥ 570 Ω/□ with and without SiO₂ surface passivation layers. Closed symbols are profiles of samples diffused without SiO₂ surface passivation layers, while open symbols are profiles of samples diffused with SiO₂ surface passivation layers. (For interpretation of the references to colour in this figure legend, the reader is referred to the Web version of this article.)

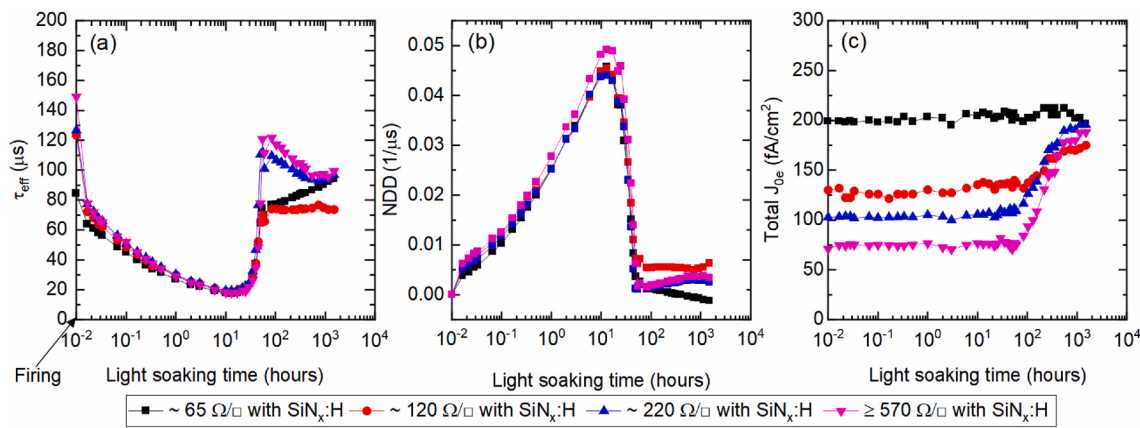


Fig. 3. Evolution of (a) effective lifetime measured at $\Delta n = 7.5 \times 10^{14}/\text{cm}^3$, (b) normalized defect density of effective lifetime and (c) total emitter saturation current density of mc-Si samples various diffused surface with emitter sheet resistance ranging from $\sim 65 \Omega/\square$ to $\geq 570 \Omega/\square$ capped with $\text{SiN}_x:\text{H}$ layers.

3.2. Impact of various emitter doping profiles with $\text{SiO}_2/\text{SiN}_x:\text{H}$ on degradation

The above section showed that controlling surface diffusion profiles passivated with $\text{SiN}_x:\text{H}$ films had no significant impact on the extent of BRD; however, it did substantially influence the extent of SRD. This section investigates how the use of a $\text{SiO}_2/\text{SiN}_x:\text{H}$, compared to a single $\text{SiN}_x:\text{H}$, influences both. Fig. 4 shows the evolution of effective lifetime, NDD and J_{oe} of samples with $\text{SiO}_2/\text{SiN}_x:\text{H}$ passivation layers. Using $\text{SiO}_2/\text{SiN}_x:\text{H}$ surface passivation had a minimal impact on the extent of BRD but considerably increased the extent of SRD. Again, the first degradation/regeneration phase was driven by the formation of a bulk defect (likely LeTID). After ~ 10 h of light soaking, all samples dropped to a similar value ($\sim 20 \mu\text{s}$), then gradually recovered to close to their initial values after ~ 60 h of light soaking. During this phase, J_{oe} remained stable (insignificant change). At the maximum bulk degradation point (~ 10 h), the NDD was $\sim 4 \times 10^{-2}/\mu\text{s}$, see Fig. 4 (b), which is very similar to the value of $\sim 4.7 \times 10^{-2}/\mu\text{s}$ for the samples without the surface oxide layer. This indicates that for these samples, the addition of a surface oxide layer had an insignificant impact on the extent of BRD.

Regarding the degradation of surface, for sheet resistances up to $\sim 240 \Omega/\square$, there was very little difference in the absolute J_{oe} increase observed on samples passivated with $\text{SiO}_2/\text{SiN}_x:\text{H}$ compared to $\text{SiN}_x:\text{H}$ alone. After long term light soaking, the J_{oe} of a sample with $R_{\text{sheet}} \sim 85 \Omega/\square$ remained unchanged, while samples with $R_{\text{sheet}} \sim 140 \Omega/\square$ and $\sim 240 \Omega/\square$, J_{oe} rose by $\sim 30 \text{ fA}/\text{cm}^2$ and $\sim 70 \text{ fA}/\text{cm}^2$, respectively, see

Fig. 4 (c). However, due to the lower starting J_{oe} values for samples with a $\text{SiO}_2/\text{SiN}_x:\text{H}$, the relative increase was much more significant for samples with $R_{\text{sheet}} \sim 240 \Omega/\square$ ($\sim 220\%_{\text{rel}}$), see Fig. 5. For the sample with the lightest emitter ($\geq 870 \Omega/\square$), both absolute ($\sim 440 \text{ fA}/\text{cm}^2$) and relative increase in J_{oe} ($\sim 1950\%_{\text{rel}}$) was substantially higher than that of the sample with $R_{\text{sheet}} \geq 570 \Omega/\square$. This is in line with previous results on undiffused samples where a greater extent of surface degradation was observed in the presence of an oxide interlayer [21,26].

There are two plausible explanations for why more SRD was observed on samples with a very light emitter capped with $\text{SiO}_2/\text{SiN}_x:\text{H}$ than on samples with $\text{SiN}_x:\text{H}$ alone. The first is that the change in doping profile during oxidation leads to a more lightly doped emitter, and hence worse recombination when defects are introduced into that region due to higher minority carrier densities. When a similar number of defects are introduced into a doped region, we would expect to see a similar absolute increase in J_{oe} irrespective of the starting point [52–54]. This was observed in the results seen in Fig. 5 for emitter profiles with R_{sheet} between $\sim 65 \Omega/\square$ and $\sim 220 \Omega/\square$. However, it may clearly be seen that the extent of this change was far more pronounced for the most lightly doped samples ($R_{\text{sheet}} \geq 570 \Omega/\square$), which show a significant difference in the absolute and relative change in J_{oe} . This might indicate that the $\sim 20 \Omega/\square$ increase in sheet resistance observed on samples with initial $R_{\text{sheet}} < 220 \Omega/\square$ due to oxidation did not noticeably alter the number of defects generated, whereas there was a significant increase in defect generation due to the $300 \Omega/\square$ change in R_{sheet} for the most lightly doped emitter.

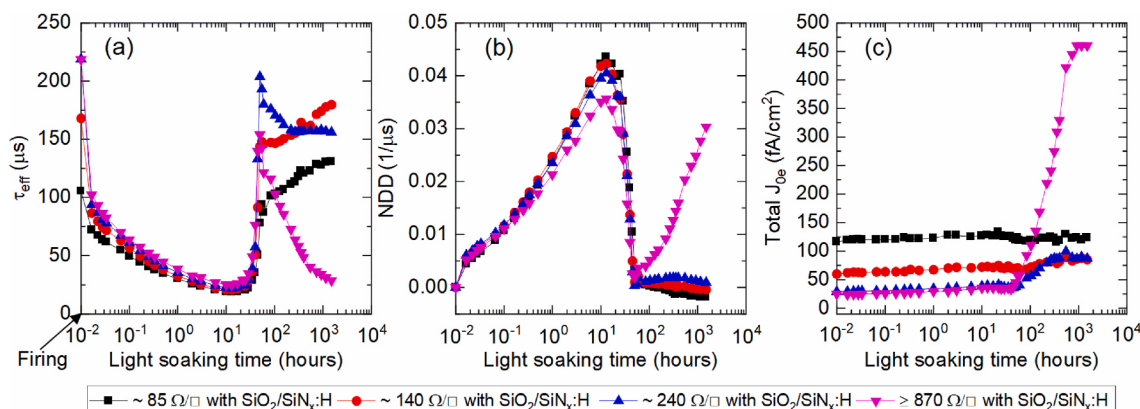


Fig. 4. Evolution of (a) effective lifetime measured at $\Delta n = 7.5 \times 10^{14}/\text{cm}^3$, (b) normalized defect density of effective lifetime and (c) total emitter saturation current density of mc-Si diffused with various R_{sheet} ranging from $\sim 85 \Omega/\square$ to $\geq 850 \Omega/\square$ capped with $\text{SiO}_2/\text{SiN}_x:\text{H}$ surface passivation layers on both sides. Note that the introduction of thermal SiO_2 reduced surface doping concentration, led to an increase in R_{sheet} by $\sim 20 \Omega/\square$ for samples with the prior $R_{\text{sheet}} \sim 65 \Omega/\square$ to $\sim 220 \Omega/\square$ and $\sim 300 \Omega/\square$ for samples with the prior $R_{\text{sheet}} \geq 570 \Omega/\square$.

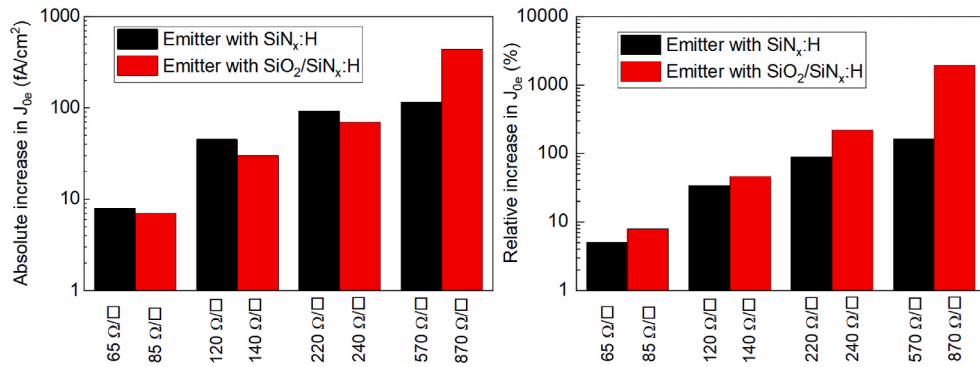


Fig. 5. Summary of the absolute (a) and (b) relative increase in J_{0e} after ~ 2000 h of mc-Si with emitter variation with $\text{SiN}_x\text{:H}$ and $\text{SiO}_2/\text{SiN}_x\text{:H}$ passivation layers.

A second possibility is that SRD in samples with an oxide layer is exacerbated by the simultaneous formation of recombination active defects and a loss of fixed dielectric charge. In previous work, Sperber et al. identified that during SRD, wafers passivated with $\text{SiN}_x\text{:H}$ layers experienced a loss in chemical passivation (formation of defects) with no loss of fixed charge, while those passivated with $\text{Al}_2\text{O}_3/\text{SiN}_x\text{:H}$ saw a significant decrease in fixed surface charge, with a slight improvement in chemical passivation [26]. Recent work by Tan observed both a decrease in chemical passivation and a loss of fixed charge on undiffused Cz-Si samples passivated with $\text{SiO}_2/\text{SiN}_x\text{:H}$ layers during SRD [21]. This may indicate that the thin interfacial SiO_2 layer found in most Al_2O_3 dielectrics plays a role in this loss of fixed charge. However, it is worth pointing out that in the case of $\text{Al}_2\text{O}_3/\text{SiN}_x\text{:H}$, a reduction in fixed negative charge was observed during SRD, while for $\text{SiO}_2/\text{SiN}_x\text{:H}$, there was a reduction in fixed positive charge.

There is no evidence in our results to support the loss of fixed surface charge in addition to defect generation for samples with emitter peak doping of $1 \times 10^{19} \text{ cm}^{-3}$ or above. Assuming the same number of defects were generated for samples with and without an oxide, a loss of fixed surface charge for samples with a SiO_2 interlayer would be expected to lead to an observable increase in both absolute and relative J_{0e} rise when compared to samples without SiO_2 . This rise would be greatest for sheet resistances $> 200 \Omega/\square$ but should still be observable for samples with $R_{sheet} > 100 \Omega/\square$, particularly given the lower peak doping in oxidized samples. There is insufficient evidence to comment either way on whether the samples with $R_{sheet} \geq 870 \Omega/\square$, experience a loss of surface charge or whether the increase in recombination is purely due to the lighter doping.

Given previous results [21], the best available explanation is that p-type samples with a $\text{SiO}_2/\text{SiN}_x\text{:H}$ stack experience an additional loss in fixed surface charge when undoped, and do not when doped with a peak concentration $> 1 \times 10^{19} \text{ cm}^{-3}$. The actual peak doping at which the loss in fixed charge is suppressed is a matter for further investigation, along with the actual mechanisms of this loss.

4. Influence of substrate materials

As presented above, modifying surface diffusion profiles and passivation layers modulated the extent of surface-related degradation in mc-Si wafers. Therefore, it is worth expanding this study onto Cz-Si substrates since this material currently dominates the solar cell market [1]. For this study, only two diffusion profiles were selected: $R_{sheet} \sim 120 \Omega/\square$ and $R_{sheet} \geq 570 \Omega/\square$. These selected conditions were based on the emitter sheet resistance currently used in the industry for a homogenous n⁺ emitter ($R_{sheet} \sim 120 \Omega/\square$), and the worse SRD observed on the mc-Si wafers with $R_{sheet} \geq 570 \Omega/\square$. In this experiment, p-type Cz-Si wafers with a resistivity of 1.7 $\Omega \text{ cm}$ were used. All Cz-Si wafers were diffused with $R_{sheet} \sim 120 \Omega/\square$, and $R_{sheet} \geq 570 \Omega/\square$, capped with $\text{SiN}_x\text{:H}$ and/or $\text{SiO}_2/\text{SiN}_x\text{:H}$ surface passivation layers on both sides, followed by firing and a stability test using the same process conditions

as summarized in Fig. 1. The stability testing results (changes in τ_{eff} , NDD, τ_{SRH} , and J_{0e} as a function of light soaking duration) of these samples are illustrated in Fig. 6. Again, it is noted that in the case of samples with $\text{SiO}_2/\text{SiN}_x\text{:H}$ surface passivation layers, the emitter sheet resistance increased from $\sim 120 \Omega/\square$ to $\sim 140 \Omega/\square$ and from $\geq 570 \Omega/\square$ to $\geq 870 \Omega/\square$ due to the introduction of the thermal oxidation process.

Varying emitter sheet resistance and surface passivation types also significantly impacted the degradation behaviour of Cz-Si wafers. All Cz-Si samples experienced the degradation/recovery of bulk (see Fig. 6 (c)) and then a secondary degradation attributed to SRD, see Fig. 6 (d). The first degradation reached its maximum degradation point after ~ 10 min of light soaking, followed by partial recovery ($\sim 50\%$ to $\sim 75\%$ of the initial lifetime), see Fig. 6 (a) and (c). After 10 min of light soaking, τ_{eff} of samples with $\text{SiN}_x\text{:H}$ layers dropped by $\sim 60 \mu\text{s}$ (NDD $\sim 6 \times 10^{-3} \mu\text{s}$) for $R_{sheet} \sim 120 \Omega/\square$, and $\sim 30 \mu\text{s}$ (NDD $\sim 6.5 \times 10^{-3} \mu\text{s}$) for $R_{sheet} \geq 570 \Omega/\square$, see Fig. 6 (a) and (b). For Cz-Si samples passivated with $\text{SiO}_2/\text{SiN}_x\text{:H}$ layers, τ_{eff} degraded by $\sim 115 \mu\text{s}$ (NDD $\sim 6.7 \times 10^{-3} \mu\text{s}$) for $R_{sheet} \sim 140 \Omega/\square$ and $\sim 470 \mu\text{s}$ (NDD $\sim 6 \times 10^{-3} \mu\text{s}$) for $R_{sheet} \geq 870 \Omega/\square$. The extent of bulk degradation of all samples was approximately the same (NDD $\sim 6\text{--}7 \times 10^{-3} \mu\text{s}$), indicating that controlling the surface diffusion profiles and passivation layers did not significantly impact the BRD extent in Cz-Si wafers. The BRD observed in Cz-Si wafers could be due to either LeTID and/or boron-oxygen related degradation (BO-LID) [55]. However, by comparing the degradation/regeneration kinetics to other studies [56,57], it is highly likely in this case that it was BO-LID.

For most Cz-Si samples, the surface started to degrade (J_{0e} increased) after ~ 10 h of light soaking, except the sample with $R_{sheet} \geq 870 \Omega/\square$ passivated with $\text{SiO}_2/\text{SiN}_x\text{:H}$, where J_{0e} rose after just ~ 1 h of light soaking. This suggests that the surface of this structure was very unstable, see Fig. 6 (d). The trend of SRD (measured by the percentage change of J_{0e}) in Cz-Si samples was also the same as that of mc-Si wafers, where the magnitude increased with an increasing emitter sheet resistance. The absolute increase in J_{0e} ($\sim 115 \text{ fA/cm}^2$) for heavy diffused samples with oxide was also lower, but the relative change in J_{0e} ($\sim 180\%_{rel}$) was higher than samples without oxide (absolute $\sim 230 \text{ fA/cm}^2$ and relative $\sim 160\%_{rel}$). However, for the lightly doped emitter, both terms were greater for samples with an oxide interlayer. The J_{0e} of the sample with $R_{sheet} \geq 570 \Omega/\square$ (without oxide) increased by $\sim 550 \text{ fA/cm}^2$ ($\sim 230\%_{rel}$), while for the sample with $R_{sheet} \geq 870 \Omega/\square$ (with oxide), J_{0e} increased by $\sim 1080 \text{ fA/cm}^2$, which is equivalent to $\sim 4500\%_{rel}$.

Notably, the model used for fitting the measured effective lifetime could not account for the contribution of recombination associated with the observed SRD behaviour (light-soak durations beyond the recovery of BRD). As this model assumes only two possible recombination components, that of typical surface recombination occurring directly at the metal-silicon interface and SRH-type bulk recombination far away from this interface, thus an increasingly unreliable estimation of SRH bulk lifetime was obtained within the SRD expression phase. This may

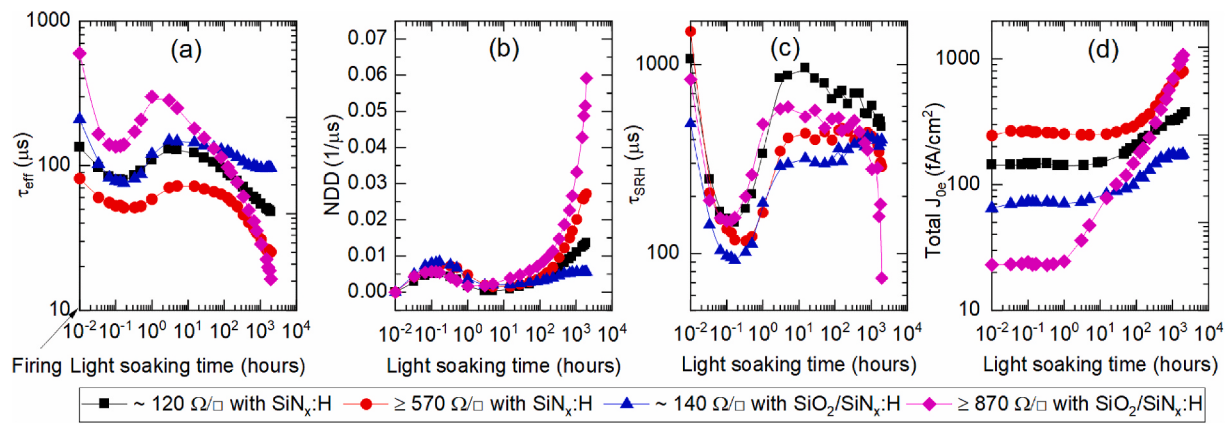


Fig. 6. Evolution of (a) effective lifetime measured at $\Delta n = 8.5 \times 10^{14}/\text{cm}^3$, (b) normalized defect density of effective lifetime, (c) SRH related bulk lifetime, and (d) total emitter saturation current density of the Cz-Si samples with $R_{\text{sheet}} \sim 120 \Omega/\square$ and $\geq 570 \Omega/\square$ capped with $\text{SiN}_x:\text{H}$ and $R_{\text{sheet}} \sim 140 \Omega/\square$ and $\geq 870 \Omega/\square$ capped with $\text{SiO}_2/\text{SiN}_x:\text{H}$.

indicate that SRD involves a new defect, not well described by J_{0e} alone, and this may be due to the defect occurring in a region close to but not directly at the interface. Importantly, however, this does not significantly impact the fitting and calculation of J_{0e} . Also, so far, there is no known bulk degradation mechanism at these timescales (long duration light-soak beyond the recovery of BRD).

These results appear to somewhat contradict previous observations by Sperber et al. [58], where there was no surface degradation observed on the sample diffused with an emitter sheet resistance of $\sim 120 \Omega/\square$ (J_{0e} remained relatively constant after long term light soaking). However, it should be noted that in work by Sperber et al., FZ-Si substrates were used, and the sample preparation method involved a chemical process in turning a heavy emitter ($R_{\text{sheet}} \sim 55 \Omega/\square$) into a light emitter ($R_{\text{sheet}} \sim 120 \Omega/\square$). In contrast, in this work, mc-Si and Cz-Si wafers were considered, and all samples were directly diffused to achieve target sheet resistances; these possibly account for the different observations between these two studies. In addition, it may also be possible that the extent of SRD was dependent on the surface dopant concentration rather than the actual sheet resistance. To verify this, further studies are required.

Again, it is important to point out that the initial J_{0e} of the Cz-Si sample with $R_{\text{sheet}} \geq 570 \Omega/\square$ passivated with $\text{SiN}_x:\text{H}$ ($\sim 250 \text{ fA}/\text{cm}^2$) was higher than that of the mc-Si sample with $R_{\text{sheet}} \sim 65 \Omega/\square$ capped with $\text{SiN}_x:\text{H}$ ($J_{0e} \sim 200 \text{ fA}/\text{cm}^2$) illustrated in section 3.1. However, in this case, J_{0e} still increased substantially (from $\sim 250 \text{ fA}/\text{cm}^2$ to $\sim 800 \text{ fA}/\text{cm}^2$), implying that the stability of surface in the mc-Si sample with

$R_{\text{sheet}} \sim 65 \Omega/\square$ capped with $\text{SiN}_x:\text{H}$ was not due to its higher initial J_{0e} , but mainly due to the presence of a heavily diffused layer in the structures.

4.1. Comparing the extent of surface degradation in mc-Si and Cz-Si

To better quantify which substrate material was more susceptible to surface degradation, relative changes in J_{0e} of both substrates were regrouped according to emitter sheet resistance and types of surface passivation layers, as shown in Fig. 7. It is evident that surface degradation in Cz-Si samples was much more severe and occurred more rapidly than mc-Si wafers. SRD in Cz-Si wafers continued to increase even after ~ 2000 h of light soaking (J_{0e} kept increasing). In contrast, SRD in mc-Si wafers stopped rising after ~ 500 h. In the case of $R_{\text{sheet}} \sim 120 \Omega/\square$ (or $\sim 140 \Omega/\square$) capped with $\text{SiN}_x:\text{H}$ or $\text{SiO}_2/\text{SiN}_x:\text{H}$, J_{0e} of the Cz-Si samples increased by approximately three times higher than that of the mc-Si samples. For the structure with $R_{\text{sheet}} \geq 570 \Omega/\square$ passivated with $\text{SiN}_x:\text{H}$, J_{0e} increased by $\sim 230\%_{\text{rel}}$ for Cz-Si, but only $\sim 160\%_{\text{rel}}$ for the mc-Si samples. The most extreme case was realized on the sample with a very light emitter ($R_{\text{sheet}} \geq 870 \Omega/\square$) capped with $\text{SiO}_2/\text{SiN}_x:\text{H}$, where J_{0e} increased by $\sim 4500\%_{\text{rel}}$ for Cz-Si, while only $\sim 2000\%_{\text{rel}}$ for mc-Si samples. If this degradation is caused by a build-up of excess hydrogen atoms, then the greater extent of SRD observed on Cz-Si compared to mc-Si substrates might be explained by the structural difference between the materials. The presence of lower concentrations of impurities and structural defects (grain boundaries, dislocation clusters)

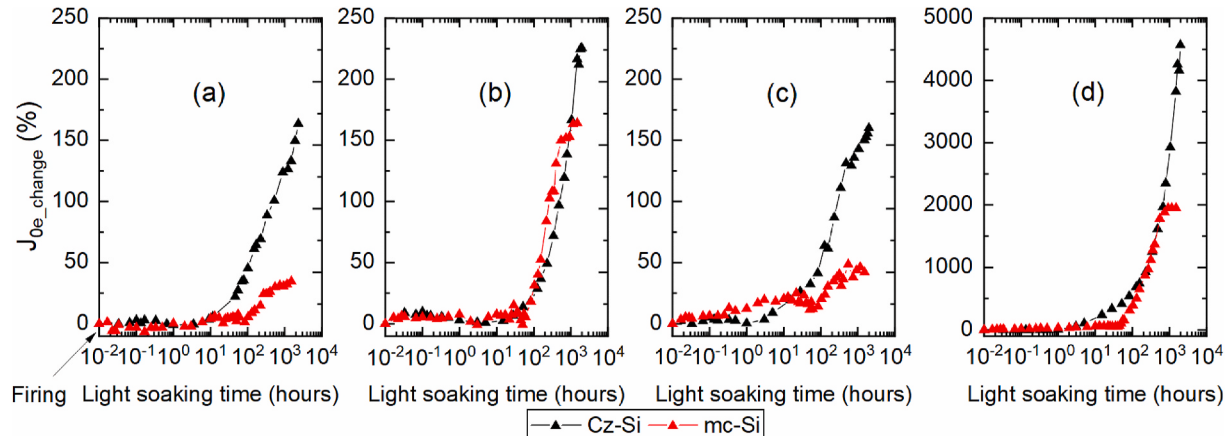


Fig. 7. Comparing relative changes in J_{0e} of the mc-Si and the Cz-Si samples with (a) $R_{\text{sheet}} \sim 120 \Omega/\square$ passivated with $\text{SiN}_x:\text{H}$, (b) $R_{\text{sheet}} \geq 570 \Omega/\square$ passivated with $\text{SiN}_x:\text{H}$, (c) $R_{\text{sheet}} \sim 140 \Omega/\square$ passivated with $\text{SiO}_2/\text{SiN}_x:\text{H}$, and (d) $R_{\text{sheet}} \geq 870 \Omega/\square$ passivated with $\text{SiO}_2/\text{SiN}_x:\text{H}$.

in Cz-Si may accelerate free hydrogen moving to the surface after debonding from the bulk defects (rather than being trapped in those sites in the mc-Si wafers). As a result, surface recombination in Cz-Si structures begins quicker and is more pronounced than the mc-Si test structures. These results could further suggest a more pronounced SRD in the FZ-Si than the Cz-Si wafer. However, this implication seems to contradict Sperber's work [58], where no SRD was observed in FZ-Si wafers with similar structures. It remains unclear why this is the case, but as mentioned earlier, the emitter sheet resistance achieved in both works was different; this might lead to a different outcome. Replicating this experiment on FZ-Si wafers is required in the future to pinpoint the root cause of the dissimilarity.

These results highlight the higher potential for severe SRD in Cz-Si solar cells compared to mc-Si solar cells, suggesting that a more detailed study is needed for Cz-Si based solar cells, particularly for the cell architectures that incorporate a SiO₂ layer into the structures.

5. Impact of undiffused passivation layers on rear side surface degradation

The results on the symmetrical lifetime test structures above showed that the introduction of SiO₂/SiN_x:H surface passivation layers led to more significant front side surface degradation. It has also been reported that PERC cells capped with SiO₂/SiN_x:H rear passivation layers are substantially impacted by surface degradation at the rear side [29]. Therefore, the role of various rear passivation layers in modulating the extent of SRD in PERC precursors was investigated. In this study, p-type mc-Si ($1.8 \Omega \text{ cm}$) PERC precursors capped with various rear passivation layers were created on the industrial pilot line at Canadian Solar. For this group, all wafers were textured, RCA cleaned, then underwent phosphorus diffusion to achieve a front emitter sheet resistance of $\sim 100 \Omega/\square$, followed by an edge isolation step using the industry-standard recipes. Then, a SiN_x:H passivation layer ($\sim 85\text{-nm-thick}$) was introduced to the front surface of all samples. Subsequently, a range of rear passivation layers was deposited, as detailed in Fig. 8. The Al₂O₃ layers were deposited using atomic layer deposition (ALD), and both front and rear SiN_x:H layers were deposited with PECVD using standard industrial

recipes. After deposition of rear passivation layers, all samples were fired, followed by stability testing at 130°C , 1000 W/m^2 . The SiO₂ layers were grown via thermal process with industry recipes.

Fig. 9 displays the changes of τ_{eff} , NDD and J_{0e} of the mc-Si PERC precursors capped with different rear passivation layers. Similar to the results of the lifetime test structures discussed above, the first degradation/regeneration phase was due to BRD (likely LeTID), and the second degradation was due to SRD. Interestingly, surface degradation was only found on samples using SiO₂/SiN_x:H rear passivation layers. The J_{0e} of the PERC precursors coated with SiO₂/SiN_x:H rear passivation layers (both 10-nm-thick and 20-nm-thick) increased by $\sim 100 \text{ fA/m}^2$ after $\sim 3000 \text{ h}$ of light soaking. However, the J_{0e} of the samples passivated with Al₂O₃/SiN_x:H rear layers remained constant after the same stability testing duration, regardless of the thickness of the Al₂O₃ and SiN_x:H films, see Fig. 9 (c). The results in the previous section demonstrated that no SRD is expected to occur in the emitter region of these structures. Therefore, we assume that the surface degradation observed on the samples with undiffused SiO₂/SiN_x:H rear passivation layers in this section is caused by increasing recombination at the rear surface region rather than the front surface. These results also agreed with previous observations that the introduction of SiO₂/SiN_x:H surface passivation layers led to more pronounced surface degradation on symmetric lifetime structures. These results also aligned with Herguth et al.'s work, demonstrating surface degradation on the Cz-Si PERC cells incorporating SiO₂/SiN_x:H rear passivation layers.

Accounting for all the reports in the literature, the case of surface degradation in samples passivated with Al₂O₃/SiN_x:H stacks is complex, with some reports observing a loss in fixed charge [26], while others see minimal change in surface recombination [59]. Since the number of studies to date is small, it is not yet clear if these differences are simply a result of light soaking at different temperatures or variations in the susceptibility of different stacks. The lack of degradation at the Al₂O₃/SiN_x:H passivated surfaces in this work could thus be attributed to three possible causes:

- 1) The industrial Al₂O₃/SiN_x:H stacks used in this work are not susceptible to a loss in fixed charge.

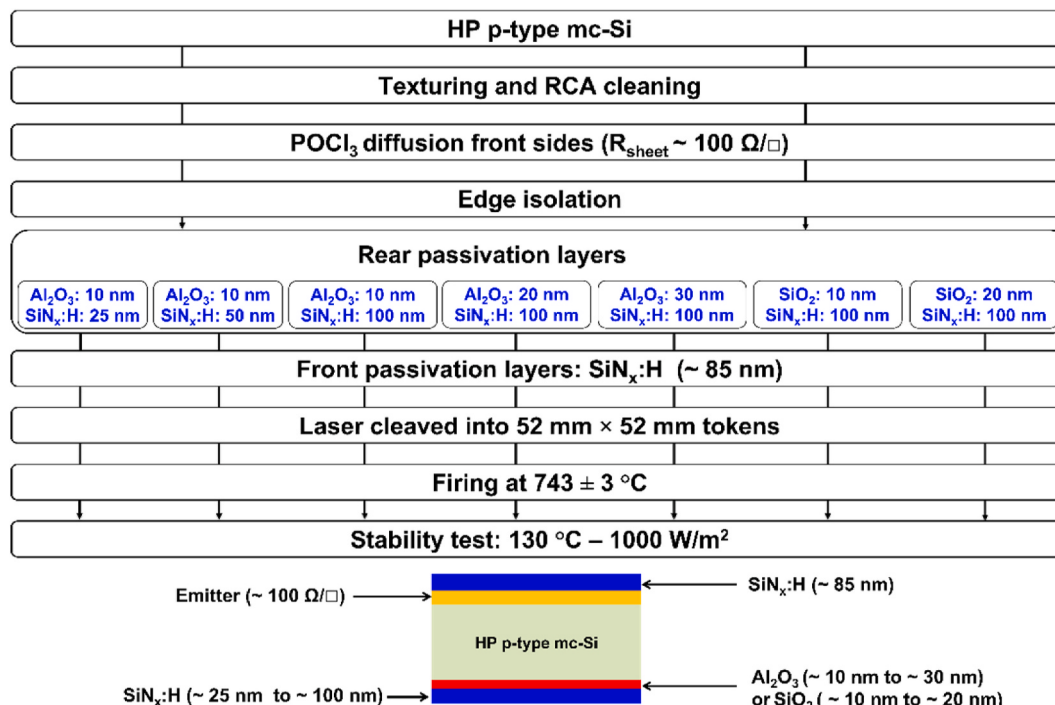


Fig. 8. Experiment flow diagram (top) and sample structures (bottom) to study the impact of rear passivation layers on surface degradation.

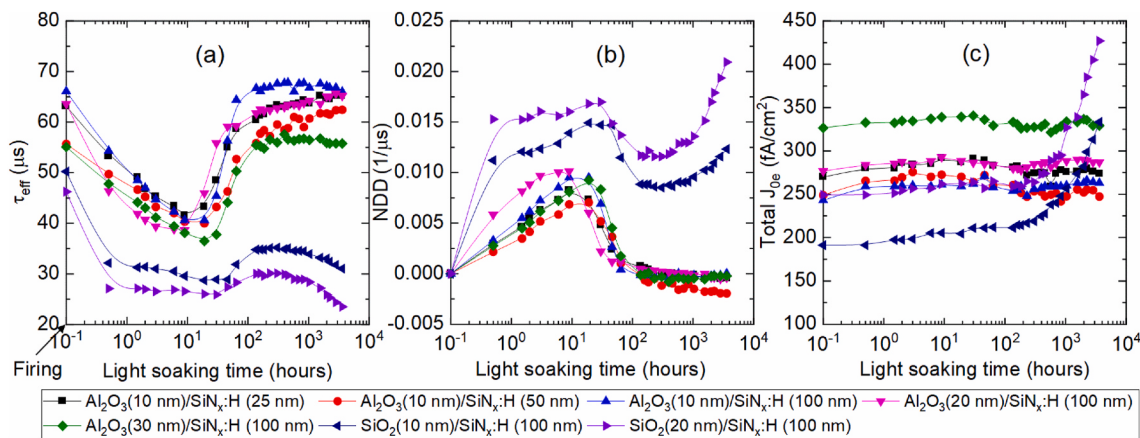


Fig. 9. Evolution of (a) effective lifetime measured at $\Delta n = 8 \times 10^{14}/\text{cm}^3$ (b) normalized defect density of effective lifetime and (c) emitter saturation current density as a function of the light soaking duration of mc-Si samples capped with various rear passivation layers.

- 2) The use of a non-symmetrical structure with a diffused emitter at the front surface alters the distribution of H in the device.
- 3) As opposed to Cz- or FZ-Si, the use of mc-Si substrate reduces the extent such that it does not affect the Al₂O₃/SiN_x:H passivated surfaces.

This is an area that requires further research and may help develop an understanding of how SRD manifests on different types of surfaces.

Overall, the results in this work demonstrate that surface-related degradation is not expected to impact mc-Si PERC cells coated with Al₂O₃/SiN_x:H films on the rear side. However, careful attention must be paid to architectures that use a SiO₂ surface passivation layer, such as TOPCon, particularly for n-type Cz-Si wafers, as it has already been demonstrated by Chen et al. that SRD in n-type Cz-Si occurs more rapidly and more severely than that of p-type wafers [31].

It should be noted that all samples were significantly impacted by BRD. This was highly likely due to LeTID defects considering the degradation/regeneration kinetics, as also observed in our earlier study [3]. The greatest BRD extent was observed on the samples passivated with SiO₂/SiN_x:H rear layers ($\text{NDD} \sim 15 \times 10^{-3}/\mu\text{s}$), see Fig. 9 (b). This is likely due to the impact of the Al₂O₃ film, which acted as a barrier layer reducing hydrogen released into the bulk from the SiN_x:H in the rear surface during the firing process, as suggested by Varshney et al. and Wilking et al. [60,61]. For samples capped with different thicknesses of either Al₂O₃ or SiN_x:H films, no clear trend of BRD ($\text{NDD} \sim 7 \times 10^{-3}/\mu\text{s}$) was observed. These results contrast those presented by Schmid et al. [62], demonstrating a reduction in the extent of LeTID with increasing thickness of the Al₂O₃ passivation layer. However, in work by Schmid et al., Al₂O₃ films were introduced to both sides of samples, but Al₂O₃ films were only used for rear passivation in this work. Therefore, it might be expected that the bulk of the hydrogen in the structure comes from the SiN_x:H layers on the front of the cell precursors.

6. Conclusion

This work investigated the roles of several key photovoltaic cell design parameters on the extent of light-induced degradation of both the bulk and surface in lifetime test structures and PERC precursors. This included variations in the n⁺ emitter layers, surface dielectrics with and without thermal oxides, the substrate material, and rear passivation layers. It was found that increasing the emitter sheet resistance of the diffused layers (moving toward lightly doped emitters) had a minimal impact on bulk degradation but elevated the extent of surface degradation. This is suspected to be related to an alteration in the behaviour of hydrogen in the surface regions with varying diffusion profiles. The

introduction of SiO₂/SiN_x:H surface passivation was found to increase the extent of surface degradation for the case of a lightly doped emitter ($R_{\text{sheet}} \geq 870 \Omega/\square$). It was suggested that this might be due to the variation in doping profile during oxidation or the loss of fixed dielectric charge and increased defect density at the interface. Cz-Si wafers were observed to be more susceptible to SRD than mc-Si wafers, related to more impurities and/or structural defects in the mc-Si substrates acting as hydrogen traps and reducing hydrogen transport to the surface regions after bulk regeneration. The results of varying the thickness and types of rear surface passivation layers on mc-Si PERC precursors showed that surface degradation only occurred on the PERC structures that incorporated SiO₂/SiN_x:H on the rear surface, while none was observed on the PERC precursors that used Al₂O₃/SiN_x:H as rear passivation layers, regardless of the Al₂O₃ or SiN_x:H films thickness. The findings in this work are significant for silicon solar cell manufacturers, particularly for solar cell architectures that employ selective emitter designs under the non-contacted regions, which will lead to increased sheet resistance up to ~200 Ω/□ by 2030. Additionally, the result also raises concerns regarding surface-related instability issues for future silicon solar cell architectures that incorporate SiO₂ such as TOPCon solar cells.

Declaration of competing interest

The authors declare that they have no known competing financial interests or personal relationships that could have appeared to influence the work reported in this paper.

Acknowledgements

This work was supported by the Australian Government through the Australian Renewable Energy Agency (ARENA 1-A060), the Australian Centre for Advanced Photovoltaics (ACAP, 1-SRI001). The responsibility for the views, information, or advice expressed herein is not accepted by the Australian Government. The authors would like to thank Shaozhou Wang (Bill), Zhuangyi Zhou, Nino Borojevic, Ly Mai, Duc Huy Dao, and the support of the Solar Industrial Research Facility for their contributions to sample preparation.

References

- [1] ITRPV, International Technology Roadmap for Photovoltaic (ITRPV) 2020 Results, 12th, 2021.
- [2] K. Ramspeck, S. Zimmermann, H. Nagel, A. Metz, Y. Gassenbauer, B. Birkmann, A. Seidl, S.S. Ag, S. Solar, W. GmbH, Light induced degradation of rear passivated mc-Si solar cells, Proc. 27th Eur. Photovolt. Sol. Conf. Exhib. Frankfurt, Ger. (2012) 861–865.

- [3] C. Sen, C. Chan, P. Hamer, M. Wright, C. Chong, B. Hallam, M. Abbott, Eliminating light- and elevated temperature-induced degradation in P-type PERC solar cells by a two-step thermal process, *Sol. Energy Mater. Sol. Cells* 209 (2020) 110470, <https://doi.org/10.1016/j.solmat.2020.110470>.
- [4] S.W. Glunz, S. Rein, J.Y. Lee, W. Warta, Minority carrier lifetime degradation in boron-doped Czochralski silicon, *J. Appl. Phys.* 90 (2001) 2397–2404, <https://doi.org/10.1063/1.1389076>.
- [5] K. Bothe, R. Sinton, J. Schmidt, Fundamental boron-oxygen-related carrier lifetime limit in mono- and multicrystalline silicon, *Prog. Photovoltaics Res. Appl.* 13 (2005) 287–296, <https://doi.org/10.1002/pip.586>.
- [6] A. Herguth, G. Schubert, M. Kaes, G. Hahn, A new approach to prevent the negative impact of the metastable defect in boron doped CZ silicon solar cells, in: *Conf. Rec. 2006 IEEE 4th World Conf. Photovolt. Energy Conversion, WCPEC-4* vol. 1, 2007, pp. 940–943, <https://doi.org/10.1109/WCPEC.2006.279611>.
- [7] J. Schmidt, K. Bothe, Performance-limiting oxygen-related defects in silicon solar cells, *ECS Trans* 3 (2019) 285–297, <https://doi.org/10.1149/1.2355764>.
- [8] B.J. Hallam, S.R. Wenham, P.G. Hamer, M.D. Abbott, A. Sugianto, C.E. Chan, A. M. Wenham, M.G. Eadie, G.Q. Xu, Hydrogen passivation of B-O defects in Czochralski silicon, *Energy Procedia* 38 (2013) 561–570, <https://doi.org/10.1016/j.egypro.2013.07.317>.
- [9] B.J. Hallam, P.G. Hamer, S. Wang, L. Song, N. Nampalli, M.D. Abbott, C.E. Chan, D. Lu, A.M. Wenham, L. Mai, N. Borojevic, A. Li, D. Chen, M.Y. Kim, A. Azmi, S. Wenham, Advanced hydrogenation of dislocation clusters and boron-oxygen defects in silicon solar cells, *Energy Procedia* 77 (2015) 799–809, <https://doi.org/10.1016/j.egypro.2015.07.113>.
- [10] C.E. Chan, D.N.R. Payne, B.J. Hallam, M.D. Abbott, T.H. Fung, A.M. Wenham, B. S. Tjahjono, S.R. Wenham, Rapid stabilization of high-performance multicrystalline P-type silicon PERC cells, *IEEE J. Photovoltaics*, 6 (2016) 1473–1479, <https://doi.org/10.1109/JPHOTOV.2016.2606704>.
- [11] R. Eberle, W. Kwapisil, F. Schindler, M.C. Schubert, S.W. Glunz, Impact of the firing temperature profile on light induced degradation of multicrystalline silicon, *Phys. Status Solidi Rapid Res. Lett.* 10 (2016) 861–865, <https://doi.org/10.1002/pssr.201600272>.
- [12] U. Varshney, M. Abbott, A. Ciesla, D. Chen, S. Liu, C. Sen, M. Kim, S. Wenham, B. Hoex, C. Chan, Evaluating the impact of SiNx thickness on lifetime degradation in silicon, *IEEE J. Photovoltaics* 9 (2019) 601–607, <https://doi.org/10.1109/JPHOTOV.2019.2896671>.
- [13] C. Vargas, K. Kim, G. Coletti, D. Payne, C. Chan, S. Wenham, Z. Hameiri, Carrier-induced degradation in multicrystalline silicon: dependence on the silicon nitride passivation layer and hydrogen released during firing, *IEEE J. Photovoltaics*, 8 (2018) 413–420, <https://doi.org/10.1109/JPHOTOV.2017.2783851>.
- [14] F. Kersten, J. Heitmann, J.W. Müller, Influence of Al₂O₃ and SiNx passivation layers on LeTID, 32nd, Eur. Photovolt. Sol. Energy Conf. Exhib. 92 (2016) 507–509, https://doi.org/10.4229/EUPSEC20162016-2DO_2.6.
- [15] D. Bredemeier, D.C. Walter, J. Schmidt, Possible candidates for impurities in mc-Si wafers responsible for light-induced lifetime degradation and regeneration, *Sol. RRL*, 2 (2018) 1700159, <https://doi.org/10.1002/solr.201700159>.
- [16] H.C. Sio, H. Wang, Q. Wang, C. Sun, W. Chen, H. Jin, D. Macdonald, Light and elevated temperature induced degradation in p-type and n-type cast-grown multicrystalline and mono-like silicon, *Sol. Energy Mater. Sol. Cells* 182 (2018) 98–104, <https://doi.org/10.1016/j.solmat.2018.03.002>.
- [17] S. Rein, S.W. Glunz, Electronic properties of the metastable defect in boron-doped Czochralski silicon: unambiguous determination by advanced lifetime spectroscopy, *Appl. Phys. Lett.* 82 (2003) 1054–1056, <https://doi.org/10.1063/1.1544431>.
- [18] D. Sperber, A. Herguth, Instability of dielectric surface passivation quality at elevated temperature and illumination, *Energy Procedia* 92 (2016) 211–217, <https://doi.org/10.1016/j.egypro.2016.07.061>.
- [19] D. Sperber, A. Herguth, G. Hahn, Investigating possible causes of light induced degradation in boron-doped float-zone silicon, *Proc. 33rd EUPSEC* (2017) 565–568.
- [20] K. Kim, R. Chen, D. Chen, P. Hamer, A. Ciesla Nee Wenham, S. Wenham, Z. Hameiri, A. Wenham, S. Wenham, Z. Hameiri, Degradation of surface passivation and bulk in p-type monocrystalline silicon wafers at elevated temperature, *IEEE J. Photovoltaics*, 9 (2019) 97–105, <https://doi.org/10.1109/JPHOTOV.2018.2878791>.
- [21] X. Tan, Insights into the Mechanisms of Bulk and Surface Related Degradation in Monocrystalline Silicon Solar Cells, Master Thesis, 2020.
- [22] D. Chen, P.G. Hamer, M. Kim, T.H. Fung, G. Bourret-Sicotte, S. Liu, C.E. Chan, A. Ciesla, R. Chen, M.D. Abbott, B.J. Hallam, S.R. Wenham, Hydrogen induced degradation: a possible mechanism for light- and elevated temperature- induced degradation in n-type silicon, *Sol. Energy Mater. Sol. Cells* 185 (2018) 174–182, <https://doi.org/10.1016/j.solmat.2018.05.034>.
- [23] J. Schmidt, D. Bredemeier, D.C. Walter, On the defect physics behind light and elevated temperature-induced degradation (LeTID) of multicrystalline silicon solar cells, *IEEE J. Photovoltaics* (2019) 1–7, <https://doi.org/10.1109/jphoton.2019.2937223>.
- [24] J. Lindroos, H. Savin, Review of light-induced degradation in crystalline silicon solar cells, *Sol. Energy Mater. Sol. Cells* 147 (2016) 115–126, <https://doi.org/10.1016/j.solmat.2015.11.047>.
- [25] C. Sen, C. Chan, D. Chen, M. Wright, U. Varshney, M. Kim, A. Samadi, S. Liu, A. Ciesla, C. Chong, B. Hallam, M. Abbott, Different extent and behaviour of LeTID in the past and current PERC silicon solar cells, *Asia-Pacific, Sol. Res. Conf.* 2 (2019) 3–6.
- [26] D. Sperber, A. Graf, D. Skorka, A. Herguth, G. Hahn, Degradation of surface passivation on crystalline silicon and its impact on light-induced degradation experiments, *IEEE J. Photovoltaics*, 7 (2017) 1627–1634, <https://doi.org/10.1109/JPHOTOV.2017.2755072>.
- [27] D. Sperber, A. Schwarz, A. Herguth, G. Hahn, Bulk and surface-related degradation in lifetime samples made of Czochralski silicon passivated by plasma-enhanced chemical vapor deposited layer stacks, *Phys. Status Solidi* 1800741 (2018) 1–7, <https://doi.org/10.1002/pssa.201800741>.
- [28] D. Sperber, A. Graf, A. Heilemann, A. Herguth, G. Hahn, Bulk and surface instabilities in boron doped float-zone samples during light induced degradation treatments, *Energy Procedia* 124 (2017) 794–798, <https://doi.org/10.1016/j.egypro.2017.09.349>.
- [29] A. Herguth, C. Derricks, D. Sperber, A detailed study on light-induced degradation of Cz-Si PERC-type solar cells: evidence of rear surface-related degradation, *IEEE J. Photovoltaics* 8 (2018) 1190–1201, <https://doi.org/10.1109/JPHOTOV.2018.2850521>.
- [30] D. Chen, P.G. Hamer, M. Kim, T.H. Fung, G. Bourret-Sicotte, S. Liu, C.E. Chan, A. Ciesla, R. Chen, M.D. Abbott, B.J. Hallam, S.R. Wenham, Hydrogen induced degradation: a possible mechanism for light- and elevated temperature- induced degradation in n-type silicon, *Sol. Energy Mater. Sol. Cells* 185 (2018) 174–182, <https://doi.org/10.1016/j.solmat.2018.05.034>.
- [31] D. Chen, P. Hamer, M. Kim, C. Chan, A. Ciesla nee Wenham, F. Rougieux, Y. Zhang, M. Abbott, B. Hallam, Hydrogen-induced degradation: explaining the mechanism behind light- and elevated temperature-induced degradation in n- and p-type silicon, *Sol. Energy Mater. Sol. Cells* 207 (2020) 110353, <https://doi.org/10.1016/j.solmat.2019.110353>.
- [32] J.M. Fritz, A. Zuschlag, D. Skorka, A. Schmid, G. Hahn, Temperature dependent degradation and regeneration of differently doped mc-Si materials, *Energy Procedia* 124 (2017) 718–725, <https://doi.org/10.1016/j.egypro.2017.09.085>.
- [33] R.A. Sinton, A. Cuevas, Contactless determination of current-voltage characteristics and minority-carrier lifetimes in semiconductors from quasi-steady-state photoconductance data, *Appl. Phys. Lett.* 69 (1996) 2510–2512, <https://doi.org/10.1063/1.117723>.
- [34] H. Nagel, C. Berge, A.G. Aberle, Generalized analysis of quasi-steady-state and quasi-transient measurements of carrier lifetimes in semiconductors, *J. Appl. Phys.* 86 (1999) 6218–6221, <https://doi.org/10.1063/1.371633>.
- [35] A. Richter, F. Werner, A. Cuevas, J. Schmidt, S.W. Glunz, Improved parameterization of Auger recombination in silicon, *Energy Procedia* 27 (2012) 88–94, <https://doi.org/10.1016/j.egypro.2012.07.034>.
- [36] S.W. Glunz, S. Rein, W. Warta, J. Knobloch, W. Wetting, Degradation of carrier lifetime in CZ silicon solar cells, *Sol. Energy Mater. Sol. Cells* 65 (2001) 219–229, [https://doi.org/10.1016/S0927-0248\(00\)00098-2](https://doi.org/10.1016/S0927-0248(00)00098-2).
- [37] A. Cuevas, The effect of emitter recombination on the effective lifetime of silicon wafers, *Sol. Energy Mater. Sol. Cells* 57 (1999) 277–290, [https://doi.org/10.1016/S0927-0248\(98\)00179-2](https://doi.org/10.1016/S0927-0248(98)00179-2).
- [38] W. Shockley, W.T. Read, Statistics of the recombination of holes and electrons, *Phys. Rev.* 87 (1952) 835–842, <https://doi.org/10.1103/PhysRev.87.835>.
- [39] C. Sen, C. Chan, P. Hamer, M. Wright, U. Varshney, S. Liu, D. Chen, A. Samadi, A. Ciesla, C.M. Chong, B. Hallam, M. Abbott, Annealing prior to contact firing: a potential new approach to suppress LeTID, *Sol. Energy Mater. Sol. Cells* 200 (2019) 109938, <https://doi.org/10.1016/j.solmat.2019.109938>.
- [40] M.U. Khan, G. Scardera, S. Zou, D. Zhang, M. Abbott, The role of metal-catalyzed chemical etching black silicon in the reduction of light- and elevated temperature-induced degradation in P-type multicrystalline wafers, *IEEE J. Photovoltaics*, 2021, 1–7, <https://doi.org/10.1109/JPHOTOV.2021.3059426>.
- [41] C. Sen, M. Kim, D. Chen, U. Varshney, S. Liu, A. Samadi, A. Ciesla, S.R. Wenham, C. E. Chan, C. Chong, M.D. Abbott, B.J. Hallam, Assessing the impact of thermal profiles on the elimination of light- and elevated-temperature-induced degradation, *IEEE J. Photovoltaics* 9 (2019) 40–48, <https://doi.org/10.1109/JPHOTOV.2018.2874769>.
- [42] A. Otaegi, D. Skorka, A. Schmid, A. Zuschlag, J.C. Jimeno, G. Hahn, Influence of emitter layers on LETID kinetics in multicrystalline silicon, 35th, Eur. Photovolt. Sol. Energy Conf. Exhib. (2018) 1–14.
- [43] D. Sperber, Bulk and Surface Related Degradation Phenomena in Monocrystalline Silicon at Elevated Temperature and Illumination, PhD Thesis, 2019, <http://nbn-resolving.de/urn:nbn:de:bsz:352-2-af03ujroa2ux1>.
- [44] M. Mehler, A. Schmid, A. Zuschlag, M. Trempa, G. Hahn, Delay of regeneration by adding aluminum in boron doped crystalline Si, *Phys. Status Solidi* 2100603 (2021) 1–8, <https://doi.org/10.1002/pssa.202100603>.
- [45] S. Steingrube, P.P. Altermatt, D.S. Steingrube, J. Schmidt, R. Brendel, Interpretation of recombination at c-Si/SiNx interfaces by surface damage, *J. Appl. Phys.* 108 (2010), <https://doi.org/10.1063/1.3437643>.
- [46] N.H. Nickel, G.B. Anderson, J. Walker, Hydrogen-induced platelets in disordered silicon, *Solid State Commun.* 99 (1996) 427–431, [https://doi.org/10.1016/0038-1098\(96\)00283-9](https://doi.org/10.1016/0038-1098(96)00283-9).
- [47] N.M. Johnson, C. Herring, C. Doland, J. Walker, G.B. Anderson, F.A. Ponce, Hydrogen-induced platelets in silicon: separation of nucleation and growth, *Mater. Sci. Forum* 83–87 (1992) 33–38, <https://doi.org/10.4028/www.scientific.net/msf.83-87.33>.
- [48] J.-F. Lefèvre, E. Fourmond, A. Kaminski, O. Palais, D. Ballataud, M. Lemiti, A. Study of the composition of hydrogenated silicon nitride SiNx:H for efficient surface and bulk passivation of silicon, *Sol. Energy Mater. Sol. Cells* 93 (2009) 1281–1289, <https://doi.org/10.1016/j.solmat.2009.01.023>.
- [49] E. Cartier, J.H. Stathis, D.A. Buchanan, Passivation and depassivation of silicon dangling bonds at the Si/SiO₂ interface by atomic hydrogen, *Appl. Phys. Lett.* 63 (1993) 1510–1512, <https://doi.org/10.1063/1.110758>.

- [50] G. Dingemans, W. Beyer, M.C.M. Van De Sanden, W.M.M. Kessels, Hydrogen induced passivation of Si interfaces by Al₂O₃ films and SiO₂/Al₂O₃ stacks, *Appl. Phys. Lett.* 97 (2010) 2008–2011, <https://doi.org/10.1063/1.3497014>.
- [51] J. Schmidt, M. Kerr, A. Cuevas, Surface passivation of silicon solar cells using plasma-enhanced chemical-vapour-deposited SiN films and thin thermal SiO₂/plasma SiN stacks, *Semicond. Sci. Technol.* 16 (2001) 164–170, <https://doi.org/10.1088/0268-1242/16/3/308>.
- [52] K.R. McIntosh, P.P. Altermatt, T.J. Ratcliff, K.C. Fong, L.E. Black, S.C. Baker-Finch, M.D. Abbott, An examination of three common assumptions used to simulate recombination in heavily doped silicon, 28th Eur. Photovolt. Sol. Energy Conf. Exhib. (2013) 1672–1679, in: <http://www.eupvsec-proceedings.com/proceedings?paper=26301>.
- [53] K.R. McIntosh, P.P. Altermatt, A freeware 1D emitter model for silicon solar cells, *Conf. Rec. IEEE Photovolt. Spec. Conf.* 1 (2010) 2188–2193, <https://doi.org/10.1109/PVSC.2010.5616124>.
- [54] R.B.M. Girisch, R.P. Mertens, R.F. De Keersmaecker, Determination of Si-SiO₂ interface recombination parameters using a gate-controlled point-junction diode under illumination, *IEEE Trans. Electron. Dev.* 35 (1988) 203–222, <https://doi.org/10.1109/16.2441>.
- [55] M. Kim, D. Chen, M. Abbott, S. Wenham, B. Hallam, Role of hydrogen: formation and passivation of meta-stable defects due to hydrogen in silicon, *AIP Conf. Proc.* 1999 (2018), <https://doi.org/10.1063/1.5049329>.
- [56] S. Wilking, J. Engelhardt, S. Ebert, C. Beckh, A. Herguth, G. Hahn, High speed regeneration of BO-defects: improving long term solar cell performance within seconds, 9th Eur. PV Sol. Energy Conf. Exhib. (2014) 22–26.
- [57] G. Hahn, Svenja Wilking, A. Herguth, BO-related Defects: Overcoming Lifetime Degradation in Crystalline Si by Regeneration, vol. 242, 2016, pp. 80–89.
- [58] D. Sperber, A. Herguth, G. Hahn, On improved passivation stability on highly-doped crystalline silicon and the long-term stability of regenerated Cz-Si, *Sol. Energy Mater. Sol. Cells* 185 (2018) 277–282, <https://doi.org/10.1016/j.solmat.2018.05.031>.
- [59] T. Niewelt, W. Kwapił, M. Selinger, A. Richter, M.C. Schubert, Long-term stability of aluminum oxide based surface passivation schemes under illumination at elevated temperatures, *IEEE J. Photovoltaics*. 7 (2017) 1197–1202, <https://doi.org/10.1109/JPHOTOV.2017.2713411>.
- [60] U. Varshney, C. Chan, B. Hoex, B. Hallam, P. Hamer, A. Ciesla, D. Chen, S. Liu, C. Sen, A. Samadi, M. Abbott, Controlling light- and elevated-temperature-induced degradation with thin film barrier layers, *IEEE J. Photovoltaics*. 10 (2020) 19–27, <https://doi.org/10.1109/JPHOTOV.2019.2945199>.
- [61] S. Wilking, A. Herguth, G. Hahn, Influence of hydrogen on the regeneration of boron-oxygen related defects in crystalline silicon, *J. Appl. Phys.* 113 (2013), <https://doi.org/10.1063/1.4804310>.
- [62] A. Schmid, C. Fischer, D. Skorka, A. Zuschlag, G. Hahn, Reducing LETID with an adjustment of the AlOx-SiNy:H laser system, 37th, Eur. Photovolt. Sol. Energy Conf. Exhib. (2020) 156–159.